Fire Safety Journal 120 (2021) 103036

Contents lists available at ScienceDirect

Fire Safety Journal

journal homepage: http://www.elsevier.com/locate/firesaf

Ignition of wildland fuels by idealized firebrands

J. Rivera [a], N. Hernández [a], J.L. Consalvi [b], P. Reszka [c], J. Contreras [d], A. Fuentes [a,*]

[a] Departamento de Industrias, Universidad Técnica Federico Santa María, Av. España 1680, Casilla 110-V, Valparaíso, Chile
[b] Aix-Marseille Université, IUSTI/UMR CNRS 7343, 5 rue E. Fermi, 13453, Marseille, Cedex 13, France
[c] Faculty of Engineering and Sciences, Universidad Adolfo Ibáñez, Santiago, Chile
[d] Escuela de Ingeniería de Transporte, Pontificia Universidad Católica de Valparaíso, Avenida Brasil 2147, Valparaíso, Chile

ARTICLE INFO

Keywords:
Ignition delay time
Analytical solution
P_1 approximation
Porous media
Critical heat flux

ABSTRACT

Experiments were carried out in the Idealized-Firebrand Ignition Test (I-FIT), a bench scale apparatus specifically designed to test the ignition of forest fuel layers from a representative firebrand. A cylindrical heater was used to model the firebrand, which allowed to control the incident radiative heat flux on the specimen, from the critical heat flux up to 25 kW/m^2, for five different porosities of the fuel layer. Experimental ignition delay times were interpreted based on a theoretical model of the radiative heating of the fuel layer. Radiative heat transfer within the fuel layer was modeled by using the P_1 approximation. In the limit of small ignition delay times an analytical expression was derived to correlate the inverse of the ignition time to the incident heat flux. This analytical expression is used to obtain the ignition temperature and effective properties for the forest fuel layers, namely the product of the fuel volume fraction by solid fuel density and solid heat capacity. Analytical solutions were found to be consistent with experimental data and a correlation relating the inverse of the non-dimensional time-to-ignition to the non-dimensional heat flux is provided.

1. Introduction

The spotting process, where firebrands are lofted by fire-induced air flows and transported downwind to ignite spot fires ahead of the main fire front, is an important wildland fire spread mechanism, particularly in the wildland-urban interface (WUI) [1]. The spotting process can be divided into three stages: i) generation of firebrands mainly from burning vegetation or building components, ii) their subsequent transport by the fire plume and the prevailing wind, and iii) the flaming or glowing ignition of the receptive fuel beds. While limited number of studies have been conducted to characterize the size and mass distributions of firebrands generated from burning vegetation and building components [2,3], the modeling of the trajectories and burning rates of flying embers has received significant attention [4–6].

The present article focuses on the third step, namely the ignition process. Notable experimental works were those of Manzello and co-workers who deposited firebrands in either flaming or glowing state onto fuel beds [7,8]. Zvyagilskaya and Subbotin [9] developed a physically-based computational model that considered a detailed description of the physical and chemical processes and characterized the gas-phase, the solid-phase, the firebrand as well as their interaction. They showed that cylindrical firebrands with diameters ranging from 0.45 to 1.55 cm in charring state and landing vertically may ignite a litter of coniferous needles, provided that the moisture content in the litter does not exceed 11%. Ignition of fuel beds by spherical metal particles, which may be produced by arcing power lines, has also been studied [10–13].

An exhaustive review on the ignition of forest fuel beds by firebrands or hot metal particles has been published recently by Prof. Fernández-Pello [1].

The ignition process of biomass litter by firebrands is complex and depends on a significant amount of parameters. When a hot particle or firebrand lands on a porous forest fuel substrate, the contact between the particle and the substrate will likely be only at some points. Therefore, conduction between the particle and the fuel is only relevant at the points of contact, with convection and radiation dominating over the entire firebrand - fuel layer interface [14]. In the case of flaming firebrands, the magnitude radiation and convection transport is enhanced. The ignition phenomenon is consequently strongly dependent on the boundary conditions between these two elements, which include the three modes of heat transfer and the air flow field over the fuel bed. A comprehensive experimental representation of the ignition process has

* Corresponding author.
E-mail addresses: jose.rivera.12@sansano.usm.cl (J. Rivera), andres.fuentes@usm.cl (A. Fuentes).

https://doi.org/10.1016/j.firesaf.2020.103036
Received 16 January 2020; Accepted 28 April 2020
Available online 26 May 2020

not yet been accomplished because of the difficulties in quantifying these boundary conditions. Moreover, the experimental data previously cited indicates the presence of a stochastic phenomenon, and researchers mainly resort to pass and fail ignition criteria, but there is no theory that incorporates these probabilistic features. In order to develop an ignition theory similar to that of solid fuels subjected to radiant heat fluxes in fire calorimeters, which permits to characterize the phenomenon and obtain simple correlations for pencil and paper calculations for the practicing fire safety engineer, the configuration experimentally and theoretically investigated in the present study involved a vertically-oriented idealized firebrand that exchanges heat with the fuel bed only by radiation. This experimental setup allows to work with quantifiable boundary conditions, helping in the development of the theoretical model. The idealized firebrand, with a well-controlled temperature and radiative flux on the boundary of the fuel bed permits to reduce the problem to the spontaneous ignition of a fuel litter exposed to an incident radiative flux. While this approach simplifies the heating from the hot particle, it nevertheless provides an excellent repeatability of the experimental results and useful information on the transfer of radiant energy within the fuel bed.

2. Experimental methodology

2.1. Bench scale apparatus

Ignition experiments of pine needles litters were carried out on the I-FIT (Idealized Firebrand Ignition Test) bench scale apparatus (see Fig. 3). This apparatus was designed to reproduce equivalent conditions encountered by a single firebrand landing and eventually igniting a controlled wildland fuel layer. In this work, only a brief description of the I-FIT apparatus is given. A detailed description of the I-FIT can be found in Ref. [15]. As shown in the schematic of Fig. 3 the main experimental part considers the idealized cylindrical heater element which is positioned inside the forest fuel layer by means of a linear motor stage. The sample holder containing a fixed mass (with a controlled porosity) of forest fuel is positioned on an analytical scale (resolution of 0.01 mg). This set-up area is protected in order to avoid any interferences (on the scale and on the heater) due to the environment during the experiments. The sample holder section is protected by screens to eliminate external air currents, ensuring that the air flow within the fuel bed is due to natural convection. This configuration allows a high repeatability and accurate control of the incident heat flux on the boundary of the porous wildland fuel. The temperature inside the medium is also measured. A set of 5 thermocouples (type K) are evenly spaced in the radial direction of the sample holder where $\Delta r = 10$ mm, see Fig. 1b. The signals provided by the thermocouples are recorded by a data acquisition system (DAQ) during the experiment.

2.1.1. Heater characterization

The idealized firebrand corresponds to a cylindrical heater, specially built in silicon nitride by Bach RC (Germany), and has a size and geometry comprised in the range of common firebrands generated in real fires [2,3,16] ($d = 10$ mm and $l_z = 46$ mm). The design and construction were conceived in order to obtain reliable conditions, large emissivities (close to 0.9) and high heat fluxes in order to cover the full range of heat fluxes from hot to glowing to flaming particles. Note that in the case of lower incident heat fluxes (with longer ignition delay times), the long exposure durations might be unrealistic, since real firebrands delivering lower incident heat fluxes are likely to be consumed before ignition is attained. The characterization of the heater was carried out to precisely establish the incident radiative heat flux ($\dot{q}''_{inc}$) on the wildland fuel layer at different supplied voltages, to assess uncertainties and to evaluate the emitted radiative heat flux ($\dot{q}''_{emit}$) from the heater element. In order to determine the local $\dot{q}''_{inc}$, two Medtherm Schmidt-Boelter radiometers were placed at $r_i = 20$ mm (at different angles) from the axis of the heater (see Fig. 1b). These radiometers were used with the linear motor stage to locally measure the incident radiation on the surface of the wildland fuel.

After averaging $\dot{q}''_{inc}$ over the fuel bed, a linear relationship between the applied voltage to the heater and $\dot{q}''_{inc}$ was obtained [15], reaching up to 25 kW/m^2 on the forest fuel surface with deviations of only $\pm$ 0.1 kW/m^2.

2.1.2. Sample preparation

This study concerns dead and dried Monterey Pine (*pinus radiata*) needles collected from the Valparaiso region, Chile. To reduce their moisture content, the pine needles were oven-dried at 333 K at least 12 h, following the procedure reported in Mindykowsky et al. [17]. A weak percentage of free moisture was found in the samples, due to the self re-hydration process. This moisture content was less than 2% for the pine needles analyzed, independent of the environmental conditions (relative humidity $<$ 80%). Other characteristics of pine needles as density ($\rho_k = 615.3 \pm 19.8$ kg/m^3) and surface to volume ratio ($\omega_k = 3717 \pm 154$ m^{-1}), were experimentally measured following the procedure proposed by Tihay et al. [18]. The pine needles specific heat was taken as 1470 J/kgK [19]. In this study five forest fuel beds were tested. The different layers were obtained using the same sample volume (see Fig. 3) and modifying the mass of pine needles introduced randomly inside the sample holder ($r_o = 65$ mm and $l_z = 46$ mm in Fig. 3). This common procedure used by different groups [17,18,20] allows to obtain different porosities of the forest fuel bed (see Table 1). Another important aspect is the void volume, axisymmetrically built inside the forest fuel layer to carefully introduce the heater element using the linear motor stage. Fig. 3 shows that the distance between the heater axis and the inner boundary of the fuel litter is $r_i = 20$ mm. After the sample was prepared following the procedure described above, the sample holder

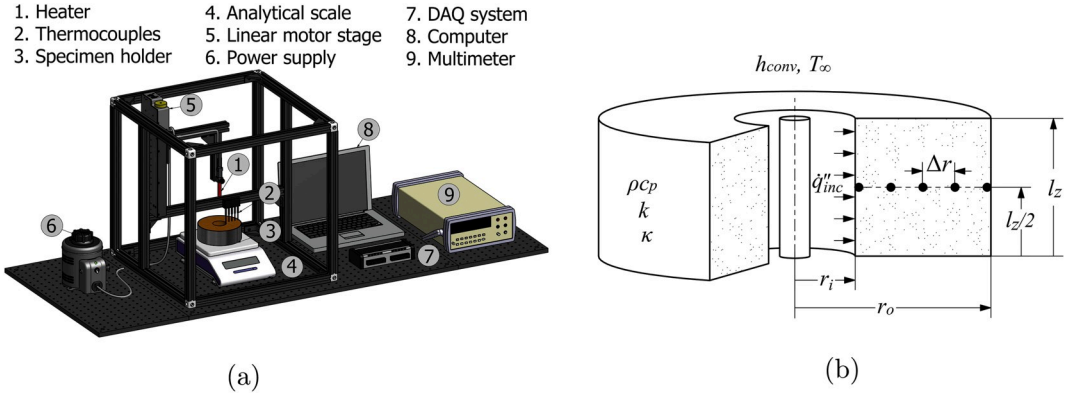

Fig. 1. (a) I-FIT bench-scale experimental setup and (b) Schematic of the equivalent medium and boundary conditions. The axis $z = 0$ is in the base of the heater and $r = 0$ is placed in the center line of the heater element.

was placed on the analytical scale perfectly aligned with the heater axis.

2.2. Experimental procedure

Prior to the commencement of the tests, steady state conditions of the heater element were assured. This was verified by heating the device and controlling the radiant heat flux by a radiometer. The time to reach steady state was 5 min for the highest voltage. In order to guarantee stable measurements for each experiment the element was heated for at least 10 min. After that, the heater was placed inside the forest fuel litter using the linear motor stage and the measurements of time to ignition, current and voltage (supplied to the heater element), mass loss and temperatures were initiated and analyzed in real-time. Time to ignition was detected by visual recognition of the flame appearance, but was also compared and validated by the evolution of the mass loss and the temperature evolution of the thermocouples placed close to the heated forest fuel layer boundary [15,17]. If ignition was attained, the heater element was extracted and the measurements were stopped when no more visual changes were observed. If ignition did not take place, measurements were stopped after 60 min. An experiment was defined by the $\dot{q}''_{inc}$ on the wildland fuel boundary and the volume fraction (α_k) of the forest fuel sample. Each experiment was repeated at least 12 times ensuring the repeatability, and the number of tests was increased close to the critical heat flux for ignition where larger deviations were normally found [15,17]. The recorded data included the time to ignition (t_{ig}), the time evolution of the radial temperatures (TC_j) and the mass (m_k) loss for different incident radiative heat fluxes on the forest fuel layer $\dot{q}''_{inc}$.

3. Theoretical approach

In order to interpret the experimental results a theoretical model is proposed. This model is based on the integral approach and the ignition temperature criterion, as they have been applied in opaque solid materials [21–23], in semi transparent cylindrical solids [24] and in porous forest fuel beds [17,20]. The boundary conditions and characteristic length of the physical problem are schematized in Fig. 1b. The resulting model is based on the following assumptions:

i. One dimensional, axisymmetrical heat transfer (*r*-axis).
ii. The forest fuel litter layer is treated as an equivalent continuous medium, the gas and solid phases being in thermal equilibrium.
iii. The solid phase remains inert during the overall heating process.
iv. Convective and diffusive heat fluxes at boundaries of the fuel layer involved are represented by an overall coefficient of heat transfer, h_{conv}.
v. The divergence of the radiative heat flux is modeled by the P_1 approximation [25].
vi. Ignition occurs when the average temperature of the medium reaches $\overline{T}_{ig}$.
vii. Effective thermal properties are used to correlate the different forest fuels tested.

3.1. Integral transform approach for heat transfer equation

Based on the above-mentioned assumptions, considering the medium temperature as $T(r,z,t)$, the energy equation is therefore given by Refs. [26,27],

$$\frac{\partial}{\partial t}\left(\alpha_k\rho_k h_k+\alpha_g\rho_g h_g\right)=\frac{1}{r}\frac{\partial}{\partial r}\left(kr\frac{\partial T}{\partial r}+k\frac{\partial T}{\partial \theta}+kr\frac{\partial T}{\partial z}-r\alpha_g\rho_g u_g h_g-r\dot{q}''_r\right)+\frac{\partial}{\partial z}\left(k\frac{\partial T}{\partial r}+\frac{k}{r}\frac{\partial T}{\partial \theta}+k\frac{\partial T}{\partial z}-\alpha_g\rho_g v_g h_g-\dot{q}''_r\right), \tag{1}$$

where $h_k=\int_{T_\infty}^{T}C_{pk}dT$, $h_g=\int_{T_\infty}^{T}C_{pg}dT$, k is the conductive coefficient, the radial, azimuthal and axial gas velocities inside the medium are represented by u_g, ω_g and ν_g respectively. On the other hand, since the enthalpy associated with the gas phase, $\alpha_g\rho_g C_{pg}$, is ~3 orders of magnitude lower than that of the solid phase, $\alpha_k\rho_k C_{pk}$, it has been neglected from the energy equation. The solution approach is based on an average temperature $\overline{T}$ for the medium defined as:

$$\overline{T}(t)=\frac{2\pi\int_0^{l_z}\int_{r_i}^{r_o}T(r,z,t)rdrdz}{2\pi\int_0^{l_z}\int_{r_i}^{r_o}rdrdz}. \tag{2}$$

Then the operator $*2/l_z(r_o^2-r_i^2)\int_0^{l_z}\int_{r_i}^{r_o}rdrdz$ is applied on both sides of Eq. (1) to work with spatially-averaged properties.

Using the continuity equation and boundary conditions at the solid fuel surface, after grouping convective and diffusive terms it is possible to obtain an overall heat transfer coefficient h_{conv}. Finally, the following simplified heat equation is obtained:

$$\alpha_k\rho_k C_{pk}\frac{\partial\overline{T}}{\partial t}=\frac{2}{r_o^2-r_i^2}\left(kr\frac{\partial T}{\partial r}-r\alpha_g\rho_g u_g h_g\right)\Big|+\frac{1}{l_z}\left(k\frac{\partial T}{\partial z}-\alpha_g\rho_g v_g h_g-\dot{q}''_r\right)\Big|_0^{l_z}-\frac{2r\dot{q}''_r}{r_o^2-r_i^2}\Big|=-\frac{h_{conv}}{l_z}(\overline{T}-T_\infty)-\frac{2(r_o\dot{q}''_r(r_o)-r_i\dot{q}''_r(r_i))}{r_o^2-r_i^2}. \tag{3}$$

Equation (3). becomes amenable to being solved analytically. The only difficulty lies in the source term related to the radiative heat flux within the porous medium. It therefore becomes necessary to introduce a model for $\dot{q}''_r(r)$ which linearizes the temperature dependence.

3.2. Radiative model

In order to obtain an expression for the radiative flux within the porous medium, the divergence of the radiative flux ($\nabla\cdot\dot{q}''_r$) was modeled based on the P_1–approximation [25] and applied to the physical problem (see Fig. 3) is the following:

$$\frac{1}{r}\frac{\partial}{\partial r}(r\dot{q}''_r)=\kappa(4\pi I_b-G) \tag{4}$$

$$\frac{\partial G}{\partial r}=-3\kappa\dot{q}''_r \tag{5}$$

$$r=r_i: G+2\dot{q}''_r=4\left(\dot{q}''_{inc}+\sigma T_\infty^4\right) \tag{6}$$

$$r=r_o: G-2\dot{q}''_r=4\sigma T_\infty^4, \tag{7}$$

where $\dot{q}''_r=\dot{q}''_r(r)$, $G=G(r)$ is the local incident radiation and σ is the Stefan-Boltzmann constant. The medium temperature is taken as the mean–volume temperature $\overline{T}$ and the surrounding temperature is T_∞. Differentiating Eq. (4) with respect to *r*,

$$\frac{\partial}{\partial r}\left(\frac{1}{r}\frac{\partial}{\partial r}(r\dot{q}''_r)\right)=-\kappa\frac{\partial G}{\partial r}, \tag{8}$$

where the absorption coefficient $\kappa=\alpha_k\omega_k/4$ [17,19] is assumed to be constant along the *r* axis. Replacing Eq. (5) into the left hand side of Eq. (8), leads to

$$\frac{\partial^2\dot{q}''_r}{\partial r^2}+\frac{1}{r}\frac{\partial\dot{q}''_r}{\partial r}-\left(3\kappa^2+\frac{1}{r^2}\right)\dot{q}''_r=0. \tag{9}$$

Eq. (9) is a modified Bessel's Equation and its general solution is given by:

$$\dot{q}''_r(r)=c_1I_1\left(\sqrt{3}\kappa r\right)+c_2K_1\left(\sqrt{3}\kappa r\right), \tag{10}$$

where I_1 and K_1 are the modified Bessel functions of first and second kind, respectively. From Eq. (6) and Eq. (7) the constants c_1 and c_2 can

be obtained. The model presented in Eq. (3.1) together with the radiative term in Eq. (10), has the form of a classical Chini's equation (see Eq. (12)). Its analytical solution is unfortunately implicit [28]. The exact solution was obtained numerically in order to compare and assess the limitations of the approximated analytical solution which is presented below.

3.3. Approximated analytical solution

In order to develop an approximated analytical solution, it is necessary to deduce the temperature at ignition (steady state conditions) for the critical incident radiative heat flux on the wildland fuel medium by replacing $\dot{q}''_{inc} = \dot{q}''_{inc,cri}$ into Eq. (6). Then,

$$-\frac{h_{conv}}{l_z}\left(\overline{T}_{ig} - T_\infty\right) - \frac{2(r_o\dot{q}''_r(r_o) - r_i\dot{q}''_r(r_i))}{r_o^2 - r_i^2} = 0, \tag{11}$$

which is solved for $\overline{T}_{ig}$ using $h_{conv} = 15$ W/m^{2}K [19]. Making algebraic manipulations in Eq. (3), the model can be written as:

$$\alpha_k\rho_k C_{pk}\frac{\partial\overline{T}}{\partial t} = -b_3 h_{conv}(\overline{T} - T_\infty) + b_1\dot{q}''_{inc} - b_2\left(\overline{T}^4 - T_\infty^4\right), \tag{12}$$

where the constants b_1, b_2 and b_3 only depend on r_i, r_o and κ. Applying a Taylor series to $T^4 - T_\infty^4 \approx 4T_\infty^3(\overline{T} - T_\infty)$ and replacing in Eq. (12), the heat equation becomes,

$$\alpha_k\rho_k C_{pk}\frac{\partial\overline{T}}{\partial t} = -b_3 h_T(\overline{T} - T_\infty) + b_1\dot{q}''_{inc}, \tag{13}$$

where $h_T = h_{conv} + 4T_\infty^3 b_2/b_3$. The following normalized variables and parameters are introduced:

$$\theta = \frac{\overline{T} - T_\infty}{\overline{T}_{ig} - T_\infty} \qquad \tau = \frac{\alpha_k\rho_k C_{pk}}{b_1\dot{q}''_{inc,cri}}\left(\overline{T}_{ig} - T_\infty\right)$$

$$\psi = \frac{b_3 h_T\left(\overline{T}_{ig} - T_\infty\right)}{b_1\dot{q}''_{inc,cri}} \qquad \phi = \frac{\dot{q}''_{inc}}{\dot{q}''_{inc,cri}} \qquad t^* = \frac{t}{\tau}.$$

Then Eq. (13) is re-written in normalized form and solved to give:

$$\theta(t^*) = \frac{\phi}{\psi}\left(1 - e^{-\psi t^*}\right), \tag{14}$$

where the initial condition $\overline{T}|_{t=0} = T_\infty \rightarrow \theta|_{t^*=0} = 0$ was applied. The approximate solution for $\overline{T}(t)$ is finally given by

$$\overline{T}(t) = T_\infty + \frac{b_1\dot{q}''_{inc}}{b_3 h_T}\left[1 - e^{-\frac{b_3 h_T t}{\alpha_k\rho_k C_{pk}}}\right]. \tag{15}$$

3.4. Correlating approach

The approximated mean temperature at ignition ($\overline{T}_{ig}$) can be easily obtained from Eq. (13) at the critical heat flux, where the mean temperature approaches steady state,

$$\overline{T}_{ig} \approx T_\infty + \frac{b_1\dot{q}''_{inc,cri}}{b_3 h_T}. \tag{16}$$

Assuming that the ignition temperature $\overline{T}_{ig}$ is a constant for all incident heat fluxes, then equating Eq. (15) with Eq. (16) gives:

$$T_\infty + \frac{b_1\dot{q}''_{inc}}{b_3 h_T}\left[1 - e^{-\frac{b_3 h_T t_{ig}}{\alpha_k\rho_k C_{pk}}}\right] = T_\infty + \frac{b_1\dot{q}''_{inc,cri}}{b_3 h_T}. \tag{17}$$

For small ignition times ($t_{ig} \rightarrow 0$) a linear relationship between $1/t_{ig}$ and $\dot{q}''_{inc}$ is obtained from Eq. (17),

$$\frac{1}{t_{ig}} \approx \left(\frac{b_3 h_T}{\alpha_k\rho_k C_{pk}\dot{q}_{inc,cri}}\right)\dot{q}''_{inc}. \tag{18}$$

From Eq. (18) it is possible to obtain effective properties for the porous wildland fuel ($\rho_k C_{pk}$) from the slope of the graph $1/t_{ig}$ vs. $\dot{q}''_{inc}$ for a specific α_k.

4. Results

4.1. Ignition delay times

The experimental results of time to ignition are presented in Fig. 2 for five different forest fuel layer porosities (see Table 1) at different incident radiative heat fluxes. The results show that the behavior is similar to spontaneous [29,30] and piloted [17,30,31] ignition measurements of wildland fuel beds carried out in different flammability apparatuses including standard fire calorimeters. As shown in Fig. 2, for a given incident heat flux, the ignition delay time increases as the fuel volume fraction decreases. For a given $\dot{q}''_{inc,}$ samples with larger α_k generate larger amounts of pyrolysis gases, which consequently induce shorter ignition delay times. The same trends have been observed for piloted ignition of forest fuel layers [17].

Uncertainties were evaluated for t_{ig} by using classical statistical procedures. The error bars plotted in Fig. 2 indicate that the uncertainty of t_{ig} decreases as the fuel volume fraction increases. For larger porosities (lower fuel volume fraction α_k), the repeatability decreased, making it necessary to increase the number of measurements in order to maintain the error within ±15%.

4.2. Critical values

The experimental campaign started from ~25 kW/m^2, decreasing systematically by steps of 2 kW/m^2 until the critical heat flux ($\dot{q}''_{inc,cri}$) was reached. In this study the critical heat flux was defined as the minimum incident radiative heat flux to obtain ignition. This value lies between the minimum heat flux associated with ignition of the specimen and the highest incident heat flux at which ignition did not occur. The bounds of this interval were then refined by dichotomy obtaining a resolution of ~0.5 kW/m^2. The observed values of $\dot{q}''_{inc,cri}$ for each α_k are presented Table 1. It can be observed that $\dot{q}''_{inc,cri}$ increases as α_k decreases. This trend was also observed in previous works involving piloted ignition in standard calorimeters [17] and numerical studies [27]. The evolution of $\dot{q}''_{inc,cri}$ is not linear with α_k and eventually decreases asymptotically for values of α_k close to a solid material.

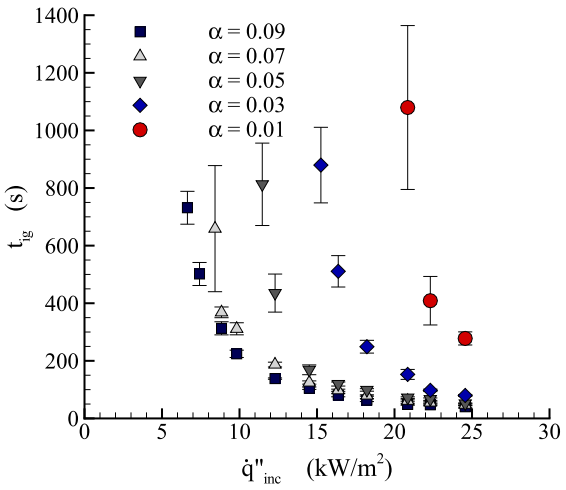

Fig. 2. Ignition delay times at different incident heat fluxes for five wildland fuel layers tested in the I-FIT apparatus.

Table 1
Comparison of effective properties obtained with the exact analytical model $(\rho_k C_{pk})^1$, the approximated analytical model $(\rho_k C_{pk})^2$ and experimentally $(\rho_k C_{pk})^3$ with the standard effective properties $(\rho_k C_{pk})^4$ for different volume fractions (α_k) of the forest fuel sample with critical heat flux and mean temperature at ignition for the forest fuel beds tested.

	m_k	$\dot{q}''_{inc,cri}$	$\overline{T}_{ig,exp}$	$\overline{T}_{ig,teo}$	$(\rho_k C_{pk})^1$	$(\rho_k C_{pk})^2$	$(\rho_k C_{pk})^3$	$(\rho_k C_{pk})^4$
	G	kW/m^2	K	K	kJ/m^{3}K	kJ/m^{3}K	kJ/m^{3}K	kJ/m^{3}K
α = 0.09	33.26	6.64	401	400	834	849	743	904
α = 0.07	25.87	8.42	443	420	936	967	812	904
α = 0.05	18.48	11.46	449	452	1037	1116	816	904
α = 0.03	11.09	15.25	460	481	1804	2115	1021	904
α = 0.01	3.70	20.85	461	489	7167	11318	4319	904

Equation (18) plots the inverse of the ignition delay time as a function of $\dot{q}''_{inc}$. Fig. 3 presents the evolution of $1/t_{ig}$ as a function of $\dot{q}''_{inc}$ for the set of experimental data. The experimental trends behave linearly for short ignition delay times, allowing to obtain effective fuel bed properties ($\rho_k c_{pk}$) from Eq. (18). These effective properties are necessary to calculate the exact solution of Eq. (12) given by Chini (continuous line) and the approximated solution (Eq. (15), dashed line). Noteworthy is the fact that for higher α_k (lower porosity), the trends of experimental data and both analytical solutions are closer to each other. This shows that the assumption of a unique spatially-averaged temperature for both the gas and solid phases becomes more precise with lower fuel layer porosity, i.e. as the porous material behaves like a homogeneous solid. On the other hand, as α_k decreases, the differences between the analytical solutions become more significant, which could be explained by linearization of radiative losses in Eq. (12). The estimated effective properties present a good match with the values of $\rho_k C_{pk}$ directly calculated with the data presented in this work, particularly for lower porosities (cf. Table 1).

4.3. Average temperature

Another way to demonstrate the ability of the proposed thermal model to describe the ignition behavior of porous fuels is to compare the evolution of the average temperature from Eq. (2) in terms of the bounds of the range of incident heat fluxes used in the experiments. While it has been shown that highly porous fuels render the assumption of a unique gas and solid phase temperature less accurate, the lack of local thermal equilibrium also becomes more significant at lower heating rates. In order to compare the experimentally estimated $\tilde{T}(t)$ and the values of $\overline{T}(t)$ obtained from the exact and approximated analytical solutions, Eq. (2) is discretized as

$$\tilde{T}(t) \approx \frac{2\sum_{j=1}^{5} T(r_j,t) r_j \Delta r}{r_o^2 - r_i^2}, \tag{19}$$

where $T(r_j,t)$ denotes the temperature measured by the thermocouple at position r_j (TC_j). The curves plotted in Fig. 4a, exhibit the results for two limit values of $\dot{q}''_{inc}$ for a fixed α_k. Note that the same behavior was observed for the specimens with different porosities. The exact solution for Eq. (12) (solid line) given by Chini shows an excellent fit with the experimental data for both of heat fluxes. As expected, the approximated analytical solution shows good agreement for large values of $\dot{q}''_{inc}$ (i.e. short t_{ig}). Another interesting result is the comparison between the experimental $\tilde{T}_{ig}$ using Eq. (19) and theoretical $\overline{T}_{ig}$ deduced from Eq. (11) (cf. Table 1), which are within ~30K. As previously explained, the use of an average temperature is less reliable for lower heat fluxes, where the magnitude of the convective losses becomes comparable to the radiative heat flux.

This analysis shows the applicability limits of the proposed model. For highly porous materials, or for low incident heat fluxes, the model fails because the magnitude of the convective losses is similar to the magnitude of the radiative heating of the porous fuel. In this case, the predictions of the ignition delay time are less accurate than the experimentally observed behavior (cf. Fig. 4a). For the case of higher heating rates or fuels approaching an homogeneous solid behavior, the ignition delay time predictions are closer to the measured values.

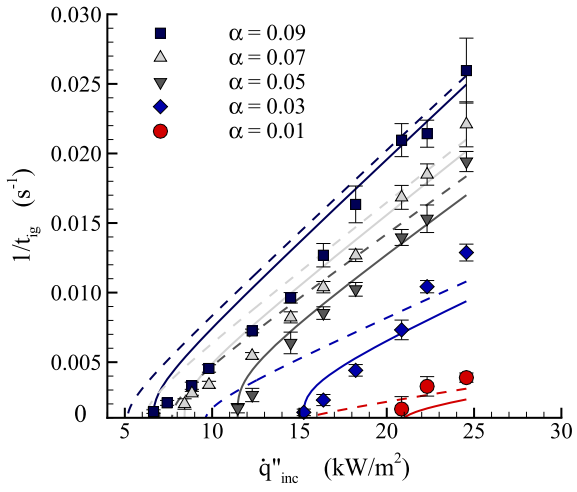

Fig. 3. Comparison between experimental (point), exact analytical (continuous line) and approximated analytical solution (dashed line) for the inverse of ignition time at different incident heat fluxes.

4.4. Correlation of results

From Eq. (14) and applying a Taylor series near $t = 0$, a useful non-dimensional relationship to correlate experimental data can be obtained, $\tau/t_{ig} \approx \phi$. Correlated experimental data are presented in Fig. 4b. Clearly, under this approach all the experimental data fit in a linear relationship, with a slope of 1.19 consistent with slope 1 deduced from $\tau/t_{ig} \approx \phi$. Although the correlation exhibits some inevitable dispersion (due to experimental conditions and medium properties), the model proposed here has potential to be used in practical forest fire safety applications to obtain quick estimates of ignition delay times of forest fuels beds based on given values of incident heat fluxes. Note that the relationship holds for a wide range of porosities, i.e. $\alpha_k = [0.01, 0.09]$.

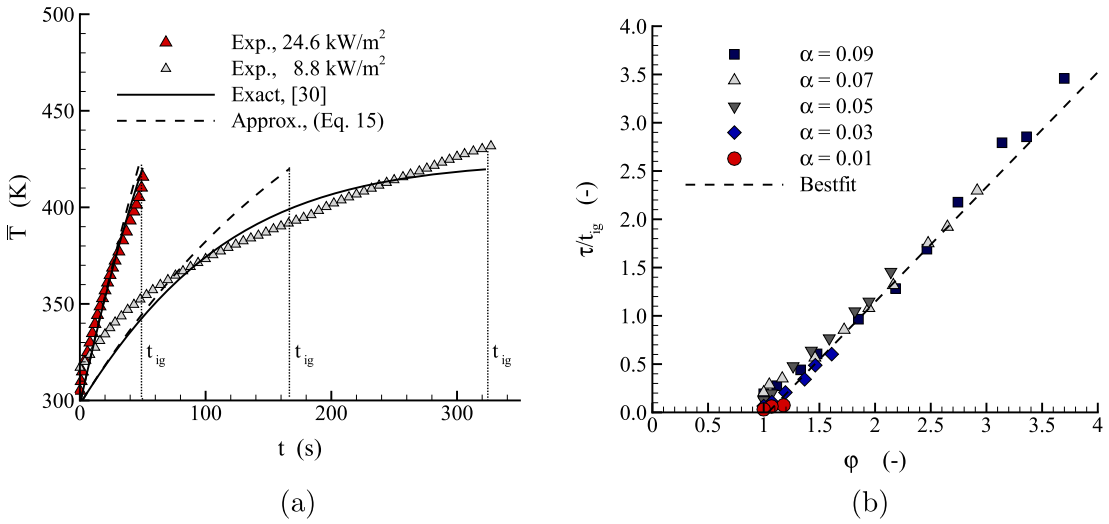

Fig. 4. (a) Evolution of average temperature, comparison between experiment, approximated analytical model and exact solution at 24.6 kW/m^2 and 8.8 kW/m^2, $\alpha = 0.07$. (b) Dimensionless ignition time for all forest fuel beds tested.

5. Conclusions

An experimental and theoretical study concerning the ignition of different forest fuel layers by idealized firebrands was carried out on a novel bench scale apparatus. The I-FIT device was specifically designed to understand the relationship between the incident radiative heat flux on the forest fuel beds and the spontaneous ignition delay time. The fuel samples tested were *pinus radiata* needles arranged in five different volume fractions (α_k) ranging from 0.01 up to 0.09, commonly encountered in wildland forest layers. A systematic and calibrated procedure was applied in order to evaluate the time to ignition under different incident heat fluxes. The measurement procedure was refined when critical heat flux was approached, assuring the repeatability and reducing the uncertainties. From the experimental results it is possible to observe that large forest fuel bed porosities require higher $\dot{q}''_{inc,cri}$ to attain ignition, similarly to previously reported piloted ignition tests.

An integral transform heat transfer equation based on the thermal equilibrium of two-phase forest fuel layers was developed. The fuel layer was considered as an absorbing and emitting medium, using a P_1 approximation for the radiative flux. Under some assumptions and by using estimated effective properties, an approximated analytical model using a spatially-averaged temperature was proposed. The predicted ignition delay times for different incident heat fluxes were compared with the exact solution, showing good potential in predicting ignition of the fuel bed. The approximated analytical model was assessed for different fuel volume fractions, from critical to large incident heat fluxes (~25 kW/m^2). The proposed model is more accurate in the cases where the convective losses are small compared to the radiant heating. This condition ceases to be valid for high fuel porosities and low incident heat fluxes. Finally, the analytical model was used to correlate non-dimensional variables for ignition time and imposed radiative heat flux allowing the estimation of effective forest fuel properties. This correlation is useful for forest fire engineering applications.

Acknowledgments

This work was funded by the National Agency for Research and Development (ANID) research programs PAI/MEC PAI80160108, PIA/ANILLO ACT172095 and Fondecyt/Regular 1191758 grants; and by DGIIP-UTFSM through the PIIC initiative

References

[1] A. Fernandez-Pello, Wildland fire spot ignition by sparks and firebrands, Fire Saf. J. 91 (1) (2017) 2–10, https://doi.org/10.1016/j.firesaf.2017.04.040.
[2] S. Manzello, A. Maranghides, W. Mell, Firebrand generation from burning vegetation, Int. J. Wildland Fire 16 (4) (2007) 458–462, https://doi.org/10.1071/WF06079.
[3] S. Manzello, J. Shields, T. Cleary, A. Maranghides, W. Mell, J. Yang, Y. H, D. Nii, T. Kurita, On the development and characterization of a firebrand generator, Fire Saf. J. 43 (4) (2008) 258–268, https://doi.org/10.1016/j.firesaf.2007.10.001.
[4] J. Woycheese, P. Pagni, D. Liepmann, Brand propagation from large-scale fires, J. Fire Protect. Eng. 10 (2) (1999) 32–44, https://doi.org/10.1177/104239159901000203.
[5] R. Anthenien, S. Tse, A. Fernandez-Pello, On the trajectories of embers initially elevated or lofted by small scale ground fire plumes in high winds, Fire Saf. J. 41 (5) (2006) 349–363, https://doi.org/10.1016/j.firesaf.2006.01.005.
[6] N. Sardoy, J. Consalvi, A. Kaiss, A. Fernandez-Pello, B. Porterie, Numerical study of ground-level distribution of firebrands generated by line fires, Combust. Flame 154 (3) (2008) 478–488, https://doi.org/10.1016/j.combustflame.2008.05.006.
[7] S. Manzello, T. Cleary, J. Shields, J. Yang, On the ignition of fuel beds by firebrands, Fire Mater. 30 (2006) 77–87, https://doi.org/10.1002/fam.901.
[8] S. Manzello, T. Cleary, J. Shields, J. Yang, Ignition of mulch and grasses by firebrands in wildland-urban interface fires, Int. J. Wildland Fire 15 (3) (2006) 417–431, https://doi.org/10.1071/WF06031.
[9] A. Zvyagils'kaya, A. Subbotin, Ignition of mulch and grasses by firebrands in wildlandurban interface fires, Combust. Explos. Shock Waves 32 (5) (1996) 558–564.
[10] G. Rowntree, A. Stokes, Fire ignition by aluminium particles of controlled size, J. Electr. Electron. Eng. 14 (1994) 117–123.
[11] C. Zak, J. Urban, A. Fernandez-Pello, Characterizing the flaming ignition of cellulose fuel beds by hot steel spheres, Combust. Sci. Technol. 186 (10–11) (2014) 1618–1631, https://doi.org/10.1080/00102202.2014.935612.
[12] J. Urban, C. Zak, J. Song, A. Fernandez-Pello, Smoldering spot ignition of natural fuels by a hot metal particle, Proc. Combust. Inst. 36 (2) (2017) 3211–3218, https://doi.org/10.1016/j.proci.2016.09.014.
[13] S. Wang, X. Huang, H. Chen, N. Liu, Interaction between flaming and smouldering in hot-particle ignition of forest fuels and effects of moisture and wind, Int. J. Wildland Fire 26 (1) (2017) 71–81, https://doi.org/10.1071/WF16096.
[14] P. Yin, N. Liu, H. Chen, J.S. Lozano, Y. Shan, New correlation between ignition time and moisture content for pine needles attacked by firebrands, Fire Technol. 50 (1) (2014) 79–91, https://doi.org/10.1007/s10694-012-0272-y.
[15] N. Hernandez, A. Fuentes, J. Consalvi, J. Elicer-Cortés, Spontaneous ignition of wildland fuel by idealized firebrands, Exp. Therm. Fluid Sci. 95 (2018) 88–95, https://doi.org/10.1016/j.expthermflusci.2018.01.037.
[16] A. Filkov, S. Prohanov, E. Mueller, D. Kasymov, P. Martynov, M. El Houssami, J. Thomas, N. Skowronski, M. Butler, B. Gallagher, K. Clark, W. Mell, R. Kremens, R. Hadden, A. Simeoni, Investigation of firebrand production during prescribed fires conducted in a pine forest, Proc. Combust. Inst. 36 (2) (2017) 3263–3270, https://doi.org/10.1016/j.proci.2016.06.125.
[17] P. Mindykowski, A. Fuentes, J. Consalvi, B. Porterie, Piloted ignition of wildland fuels, Fire Saf. J. 46 (1–2) (2011) 34–40, https://doi.org/10.1016/j.firesaf.2010.09.003.
[18] V. Tihay, A. Simeoni, P. Santoni, L. Rossi, J. Garo, J. Vantelon, Experimental study of laminar flames obtained by the homogenization of three forest fuels, Int. J. Therm. Sci. 48 (2009) 488–501, https://doi.org/10.1016/j.ijthermalsci.2008.03.018.

[19] A. Grishin, Mathematical Modeling of Forest Fires and New Methods of Fighting Them, Pub. House Tomsk University, 1986.
[20] A. Simeoni, J. Thomas, P. Bartoli, P. Borowieck, P. Reszka, F. Colella, P.-A. Santoni, J.L. Torero, Flammability studies for wildland and wildland–urban interface fires applied to pine needles and solid polymers, Fire Saf. J. 54 (2012) 203–217, https://doi.org/10.1016/j.firesaf.2012.08.005.
[21] E. Mikkola, I. Wichman, On the thermal ignition of combustible materials, Fire Mater. 14 (1989) 87–96.
[22] M. Delichatsios, T. Panagiotou, F. Kiley, The use of time to ignition data for characterizing the thermal inertia and the minimum (critical) heat flux for ignition or pyrolisis, Combust. Flame 84 (1991) 323–332, https://doi.org/10.1016/0010-2180(91)90009-Z.
[23] M. Spearpoint, J. Quintiere, Predicting the piloted ignition of wood in the cone calorimeter using an integral model – effect of species, grain orientation and heat flux, Fire Saf. J. 36 (4) (2001) 391–415, https://doi.org/10.1016/S0379-7112(00)00055-2.
[24] N. Hernández, A. Fuentes, P. Reszka, A. Fernández-Pello, Piloted ignition delay times on optically thin PMMA cylinders, Proc. Combust. Inst. 37 (3) (2019) 3993–4000, https://doi.org/10.1016/j.proci.2018.06.053.
[25] M. Modest, Radiative Heat Transfer, Academic Press, Oxford, U.K., 2013.
[26] J. Howell, Radiative transfer in porous media, in: K. Vafai (Ed.), Handbook of Porous Media, Marcel Dekker, New York, 2000, pp. 668–670. Ch. 15.
[27] J. Consalvi, F. Nmira, A. Fuentes, P. Mindykowski, B. Porterie, Numerical study of piloted ignition of forest fuel layer, Proc. Combust. Inst. 33 (2) (2011) 2641–2648, https://doi.org/10.1016/j.proci.2010.06.025.
[28] M. Chini, Sull'Integrazione di Alcune Equazioni Differenziali del Primo Ordine, Rendiconti Istituto Lombardo 57 (2) (1924) 506–511.
[29] W.M. Pitts, Ignition of cellulosic fuels by heated and radiative surfaces, Tech. Rep. 1481 (2007), https://doi.org/10.6028/nist.tn.1481. NIST.
[30] T. Fateh, F. Richard, B. Batiot, T. Rogaume, J. Louche, J. Zaida, Characterization of the burning behavior and gaseous emissions of pine needles in a cone calorimeter - ftir apparatus, Fire Saf. J. 82 (2016) 91–100, https://doi.org/10.1016/j.firesaf.2016.03.008.
[31] S. McAllister, I. Grenfell, A. Hadlow, W. Jolly, M. Finney, J. Cohen, Piloted ignition of live forest fuels, Fire Saf. J. 51 (2012) 133–142, https://doi.org/10.1016/j.firesaf.2012.04.001.